

Multi-omics analysis of immunometabolic mechanisms linking IL-33 with asthma control in children

Yingtian Yu

Affiliated Hospital of Jiangnan University

Wanying Liu

Affiliated Hospital of Jiangnan University

Tongtong Wang

Affiliated Hospital of Jiangnan University

Hui Wang

Affiliated Hospital of Jiangnan University

Xinxu Li

Affiliated Hospital of Jiangnan University

Tianzhi Chang

Jiangnan University

Dashuai Miao

Donghai County People's Hospital

Xuemei Zhou

Affiliated Hospital of Jiangnan University

Min Liu

Affiliated Hospital of Jiangnan University

Xiao Tong

dr.tong@163.com


Affiliated Hospital of Jiangnan University

Article

Keywords: IL-33, paediatric asthma, lipidomics, proteomics, membrane remodelling, endocytosis, NF- κ B

Posted Date: November 25th, 2025

DOI: <https://doi.org/10.21203/rs.3.rs-8032834/v1>

License:  This work is licensed under a Creative Commons Attribution 4.0 International License.
[Read Full License](#)

Additional Declarations: No competing interests reported.

Abstract

Background: Interleukin-33 (IL-33) is a key alarmin in paediatric asthma and is clinically associated with poor disease control and type-2 inflammation, but how IL-33 links membrane lipid remodelling, vesicular/signalling pathways and downstream immune activation in children remains unclear. We aimed to define lipidomic and proteomic signatures associated with circulating IL-33 and to relate these molecular features to asthma control and atopic burden.

Methods: We prospectively enrolled 60 children with physician-diagnosed asthma and stratified them into high- and low-IL-33 groups by serum IL-33. Untargeted serum lipidomics (n = 6 vs. 6) and label-free serum proteomics (n = 6 vs. 6) were performed on matched subsets. Differential features were identified with Benjamini–Hochberg FDR control, followed by KEGG enrichment and cross-omics integration. Associations with Asthma Control Questionnaire (ACQ) scores, total IgE and blood eosinophil percentages were assessed by Spearman correlation. A targeted qPCR panel (RELA, NFKBIA, GATA3, TBX21, PRKACA, STAM2, SPHK1, LIPE, with ADCY6, S1PR1 and ACAA1 as supplements) was used to validate the intersecting NF- κ B/Th, cAMP and endocytic pathways.

Results: Children in the high-IL-33 group had worse asthma control and higher allergic indices than those in the low-IL-33 group (ACQ \uparrow , total IgE \uparrow , eosinophils \uparrow). Lipidomics revealed a selective membrane-oriented remodelling pattern in the high-IL-33 group, characterised by increases in PC, PE and CL and a relative depletion of sphingomyelin species, with enrichment in NF- κ B signalling, Th1/Th2/Th17 differentiation and regulation of lipolysis. Proteomics showed concomitant up-regulation of endocytosis, ESCRT/vesicular transport, actin/cytoskeleton organisation, cAMP and sphingolipid signalling pathways. Cross-layer pathway overlap and correlation matrices indicated that lipid and protein changes converged on an IL-33–responsive immune axis that requires both a permissive, reconfigured membrane platform and an activated receptor-processing apparatus. qPCR findings were directionally consistent with the multi-omics results, confirming transcriptional activation of NF- κ B/Th-skewing (RELA \uparrow , GATA3 \uparrow , NFKBIA \downarrow), cAMP/ADCY6–PRKACA signalling and vesicle-related genes (STAM2 \uparrow), which in turn correlated with ACQ, IgE and eosinophilia.

Conclusions: Our data support an IL-33–lipid–transport axis in paediatric asthma, in which IL-33 elevation drives membrane-lipid remodelling (PC/PE/CL \uparrow , SM \downarrow) and parallel activation of endocytic/cAMP machinery, collectively funnelling into NF- κ B- and Th-centred inflammatory programmes that associate with poor asthma control. This composite lipid–protein–transcript fingerprint may serve as a stratification marker for IL-33-high endotypes and highlights IL-33/ST2 together with lipid-metabolic and cAMP-modulating targets as candidate therapeutic nodes.

Introduction

Asthma is the most common chronic respiratory disease in children and is marked by pronounced heterogeneity and complexity[1, 2]. While inhaled corticosteroids and bronchodilators have substantially improved symptom control for many pediatric patients, a considerable subset continues to experience

poor disease management. Epidemiological studies indicate that over 20% of children with asthma remain inadequately controlled[3–5]. Accurate assessment is therefore essential for diagnosis and standardized management, particularly in the non-exacerbation phase, where objective metrics for disease evaluation are limited[6]. In recent years, immune dysregulation and metabolic remodeling have been recognized as key determinants of phenotypic diversity and variable treatment responses in asthma[7].

Interleukin-33 (IL-33), an epithelial-derived cytokine regarded as a prototypical “alarmin,” activates innate and adaptive immunity, promotes type-2 inflammation, elevates IgE, and drives eosinophilic infiltration; its levels correlate closely with asthma severity and control[8–11]. However, how IL-33 influences pediatric asthma control through the interplay of immunity and metabolism remains insufficiently defined[12].

Lipid metabolism provides a fundamental layer of immune regulation[13, 14]. Phospholipids and sphingolipids not only constitute membrane architecture but also orchestrate receptor clustering, signal transduction, and immune-cell differentiation[15, 16]. Emerging evidence links lipid remodeling to NF- κ B and T-helper (Th1/Th2/Th17) pathways, with potential impact on asthmatic immune phenotypes[17–20]. In parallel, proteins function as effector molecules in lipid transport, vesicular trafficking, and signal modulation[21]. Advances in multi-omics now allow integrated interrogation of lipidomic and proteomic landscapes, offering new avenues to dissect asthma’s complex biology[22, 23].

In this study, we stratified children with asthma into high-IL-33 and low-IL-33 groups based on serum IL-33 concentrations and integrated lipidomic and proteomic analyses with clinical phenotypes. Our objectives were to: (i) identify lipid and protein signatures associated with IL-33 levels; (ii) delineate the key immunometabolic pathways involved; and (iii) examine the relationships between these molecular features and asthma control. We aim to elucidate the connection between IL-33–driven lipid–protein remodeling and poor asthma control in children, thereby providing a mechanistic rationale for precision assessment and targeted intervention.

Methods

Study population

We enrolled 60 pediatric outpatients with physician-diagnosed asthma (age 6–12 years) at the Affiliated Hospital of Jiangnan University. All children met GINA 2023 diagnostic criteria and were under standardized management at enrollment. Exclusion criteria were: chronic respiratory comorbidities (e.g., bronchiectasis, cystic fibrosis), acute respiratory infection within 4 weeks before enrollment, and severe systemic disease (e.g., cardiovascular disease, hepatic/renal insufficiency). The study protocol was approved by the Institutional Ethics Committee of the Affiliated Hospital of Jiangnan University (Approval No.: LS2022112). Written informed consent was obtained from legal guardians of all participants in accordance with local regulations for research involving minors.

Grouping and sampling

Peripheral venous blood (5 mL) was collected from each participant. After plasma separation, IL-33 was quantified by ELISA (R&D Systems, D3300B). Participants were dichotomized at the cohort median into High IL-33 (n = 30) and Low IL-33 (n = 30) groups. For multi-omics profiling, six samples per group (n = 6 each) were randomly selected for lipidomics (LC–MS/MS) and proteomics (TMT-based MS).

Specimen processing

Whole blood was collected in EDTA tubes and centrifuged at 3,000 rpm for 10 min at 4°C. Serum was stored at – 80°C. The cellular fraction for RNA extraction was processed within 2 h of phlebotomy. Total RNA was isolated with TRIzol (Invitrogen, USA). Lipids were extracted using a modified Bligh & Dyer method. For proteomics, lysates underwent sonication, BCA quantification, and trypsin digestion.

IL-33 quantification

ELISA was performed per the manufacturer's instructions. The standard curve covered 3.1–200 pg/mL with a lower detection limit of 1.51 pg/mL. All samples were assayed in duplicate. Absorbance at 450 nm was read on a Thermo Fisher DENLEY DRAGON Wellscan MK 3 microplate reader (Finland).

Lipidomics (UHPLC–Q Exactive Orbitrap)

Lipids Sample extraction and reconstitution

Plasma (200 µL) was transferred to a 1.5 mL microcentrifuge tube and mixed with 80 µL methanol and 400 µL MTBE. After vortexing for 30 s, samples were sonicated at 5°C, 40 kHz for 30 min, followed by a – 20°C stand for 30 min and centrifugation at 13,000 g, 4°C for 15 min. The supernatant (≈ 350 µL) was collected and evaporated to dryness under vacuum, then reconstituted in 100 µL isopropanol:acetonitrile (1:1, v/v). The mixture was sonicated in an ice–water bath (40 kHz, 5 min) and clarified by centrifugation (13,000 g, 4°C, 5–10 min); the supernatant was used for LC–MS analysis. A pooled QC sample (equal volumes from all study samples) was prepared and injected after every 10 analytical injections to monitor system stability.

LC–MS conditions

Analyses were performed on a Thermo Vanquish Horizon UHPLC coupled to a Q Exactive HF-X Orbitrap mass spectrometer. Chromatographic separation used an Accucore C30 column (100 mm × 2.1 mm, 2.6 µm) with a 2 µL injection. Mobile phase A was 10 mM ammonium acetate in ACN:H₂O = 1:1 containing 0.1% formic acid; mobile phase B was 2 mM ammonium acetate in ACN:IPA:H₂O = 10:88:2 containing 0.02% formic acid. The flow rate was 0.40 mL min^{–1} and the column temperature was 40°C. Electrospray ionization was operated in polarity-switching mode over m/z 200–2000 with spray voltage + 3000/–3000

V, sheath gas 60 arb, auxiliary gas 20 arb, and source temperature 370°C. Data were acquired in DDA mode with stepped NCE 20/40/60.

Data processing and identification

Raw files were processed in LipidSearch for baseline filtering, peak detection, retention-time alignment, peak alignment, and MS/MS-based identification. Mass tolerances were 10 ppm for both precursor and fragment ions, and identifications with confidence levels A–D were retained. Features were kept according to the 80% rule (non-zero intensity in $\geq 80\%$ of samples within at least one group), followed by minimum-value imputation, total-ion normalization, removal of features with QC-RSD $> 30\%$, and \log_{10} transformation prior to downstream analyses.

Differential analysis and enrichment.

Group separation and model stability were assessed by PCA and OPLS-DA (R package ropls, seven-fold cross-validation). Differential lipids were defined using a combined criterion of VIP > 1 (from the OPLS-DA model) and two-sided Student's t-test, $p < 0.05$. Pathway annotation and enrichment were conducted against KEGG using Fisher's exact or hypergeometric tests, with Benjamini–Hochberg FDR reported for multiple-testing control.

Proteomics (reduction–alkylation–trypsin–TMT)

Protein extraction and digestion

Plasma samples were lysed in buffer supplemented with protease inhibitors, sonicated on ice, and centrifuged at 12,000 g, 4°C for 30 min. Supernatants were quantified by BCA. Aliquots were adjusted to 100 mM TEAB, reduced with TCEP 10 mM at 37°C for 60 min, and alkylated with IAA 40 mM at room temperature in the dark for 40 min. Proteins were precipitated with 6 volumes of ice-cold acetone at -20°C for 4 h, then re-dissolved in TEAB and digested with sequencing-grade trypsin at an enzyme-to-protein ratio of 1:50 (w/w) at 37°C overnight (an additional 1:100 trypsin spike for 2 h was used when needed).

TMT labeling and LC–MS acquisition

Peptides were labeled according to the manufacturer's protocol with TMT 10-plex (or 11/16-plex where applicable). Labeled samples were pooled and, when indicated, fractionated by high-pH reversed-phase chromatography. Peptide separations were performed on an EASY-nLC 1200 (or equivalent nano-LC) coupled to an Orbitrap mass spectrometer (Fusion Lumos/Exploris or equivalent). Typical MS settings were: MS1 resolution $\geq 60,000$ (m/z 200), scan range m/z 350–1500; HCD fragmentation for reporter ion generation with MS2 resolution $\geq 15,000$ and dynamic exclusion ~ 30 s. For high-throughput runs, a 44-min method on Evosep One coupled to Orbitrap Exploris 480 was used as appropriate.

Database search and quantification

RAW files were processed in Proteome Discoverer 2.x (Sequest HT and/or MS-GF+), searching the UniProt Human database (version and download date reported in the manuscript). Enzyme specificity was Trypsin/P with up to 2 missed cleavages. Fixed modifications: Carbamidomethyl[C]; TMT-6/10-plex on peptide N-termini and Lysine. Variable modifications: Oxidation[M], protein N-terminal acetylation. Typical mass tolerances were 10 ppm (precursor) and 20 ppm (fragment), adjusted to instrument performance. Target–decoy/Percolator filtering was applied to achieve 1% FDR at PSM and protein levels. Reporter-ion quantification was performed from MS2 or (SPS-)MS3 spectra according to the acquisition strategy, followed by channel and batch normalization and appropriate missing-value handling.

Differential analysis and enrichment

Proteins showing fold change > 1.5 or < 0.67 with $p < 0.05$ were considered differentially abundant; Benjamini–Hochberg FDR was reported for multiple-testing control. Functional annotation and pathway enrichment were conducted using GO and KEGG.

qPCR validation

Selected targets (RELA, NFKBIA, GATA3, TBX21, PRKACA, STAM2, SPHK1, LIPE, ADCY6, S1PR1, ACAA1) were validated by qPCR. cDNA was synthesized using PrimeScript RT (Takara, Japan). qPCR used SYBR Green Master Mix (Applied Biosystems, USA) on an ABI 7500 Fast system. Relative expression was calculated by the $2^{-\Delta\Delta C_t}$ method with GAPDH as the internal control.

Statistical analysis

Analyses were conducted in SPSS 26.0 and GraphPad Prism 9. Between-group comparisons used independent-samples t-tests or Mann–Whitney U tests as appropriate; categorical variables used χ^2 tests. Associations were evaluated with Spearman's rank correlation. Multi-omics integration employed mixOmics (R) for canonical correlation analysis and network construction. Unless otherwise specified, two-sided tests were used and $p < 0.05$ was considered statistically significant.

Results

3.1 Clinical characteristics

A total of 60 children with asthma aged 6–12 years were enrolled and stratified by the median serum IL-33 concentration into a high-IL-33 group (High, $n=30$) and a low-IL-33 group (Low, $n=30$). There were no significant differences between groups in age, sex distribution, or body mass index (BMI) ($p>0.05$), indicating balanced baseline demographics.

Children in the high-IL-33 group exhibited significantly higher Asthma Control Questionnaire (ACQ) scores than those in the low-IL-33 group (1.71 ± 0.45 vs. 1.31 ± 0.45 , $p < 0.01$), indicating that elevated circulating IL-33 is associated with poorer asthma control (Table 1; Fig. 1A). In parallel, both total serum

IgE and peripheral blood eosinophil percentages were markedly increased in the high-IL-33 group compared with the low-IL-33 group (IgE: 225.13 ± 123.68 IU/mL vs. 136.15 ± 83.81 IU/mL, $p < 0.01$; eosinophils: 2.85 ± 1.33% vs. 1.18 ± 0.43%, $p < 0.001$), suggesting a more pronounced Th2-skewed allergic inflammatory phenotype in children with higher IL-33 levels (Table 1; Fig.1B, 1C). Moreover, FEV₁%pred was lower in the high-IL-33 group than in the low-IL-33 group (86.07 ± 6.18 vs. 90.97 ± 6.12, $p < 0.01$), further supporting a potential link between increased IL-33, impaired airway function, and suboptimal disease control (Table 1; Fig.1B–D).

Taken together, higher IL-33 levels were closely associated with poorer asthma control and with canonical Th2 inflammatory features, including elevated IgE and eosinophilic inflammation.

Table 1. Clinical features stratified by serum IL-33

Clinical parameter	Low IL-33 group (n=30)	High IL-33 group (n=30)	p-value
Age (years)	8.2 ± 1.5	8.5 ± 1.4	0.45
Sex (Male/Female)	18/12	17/13	0.79
BMI (kg/m ²)	17.8 ± 2.1	18.1 ± 2.3	0.62
ACQ score	1.31 ± 0.45	1.71 ± 0.45	<0.01
Total IgE (IU/mL)	136.15±83.81	225.13±123.68	<0.01
Peripheral eosinophils (%)	1.18±0.43	2.85±1.33	<0.001
FEV1%pred (%)	90.97 ± 6.12	86.07±6.18	<0.01

Data are presented as mean ± SD unless otherwise indicated. p-values were calculated using independent-samples t-test for continuous variables and χ^2 test for sex. ACQ, Asthma Control Questionnaire; BMI, body mass index; IgE, immunoglobulin E; FEV₁ %pred, percent predicted forced expiratory volume in 1 second.

3.2 Lipidomic analysis

3.2.1 Global profile and quality control

Untargeted serum lipidomics was performed in children stratified by IL-33 status (High, n=6; Low, n=6). Pooled quality-control (QC) injections demonstrated stable retention times and total ion current, with most QC features showing coefficients of variation <20%. After batch correction, principal component analysis (PCA) revealed clear group separation by IL-33 status (Fig 2A), indicating systematic between-group differences in lipid composition.

3.2.2 Differential lipids

Using combined thresholds (VIP > 1 and BH-FDR < 0.05), the High-IL-33 group exhibited a broad upward shift across multiple classes—most notably triglycerides (TG), cardiolipins (CL),

phosphatidylethanolamines (PE), diacylglycerols (DG), phosphatidylcholines (PC), and phosphatidylserines (PS)(Table S2). Volcano plots showed a concentration of features in the upregulated quadrant (Fig 2B), and hierarchical clustering based on significant species cleanly segregated High- and Low-IL-33 samples (Fig 2C). Within-class heterogeneity was also evident: a minority of species moved counter to the class-level trend (class-internal bidirectionality). To avoid overgeneralization from class summaries, these exceptions are catalogued in Table S1 with acyl-chain annotations and fold-change values.

3.2.3 Pathway enrichment

KEGG over-representation analysis (background: all detected lipids) identified significant enrichment of pathways related to fat digestion and absorption, regulation of lipolysis in adipocytes, NF- κ B signaling, and Th1/Th2 cell differentiation (FDR < 0.05; Fig 2D). Enrichment of fat-handling pathways supports enhanced lipid uptake and mobilization, whereas enrichment of membrane-proximal immune pathways is consistent with membrane remodeling that facilitates signal transduction. In this framework, increases in PC/PE/CL align with microdomain reorganization and receptor clustering, while elevations in DG/TG are compatible with intensified mobilization and resynthesis.

3.2.4 Associations with clinical outcomes

At the sample level, FDR-adjusted Spearman analyses linked multiple upregulated species from PC/PE/CL/TG/DG/PS to Asthma Control Questionnaire (ACQ) scores, total IgE, and peripheral eosinophil percentage (Fig 4D). At the module level, pathway scores for fat digestion and absorption and for regulation of lipolysis in adipocytes showed stronger positive associations with ACQ/IgE than other pathways, suggesting concordant variation between metabolic mobilization, membrane remodeling, and worse asthma control/allergic inflammation.

3.2.5 Robustness and sensitivity analyses

Findings were stable after (i) exclusion of outliers; (ii) sensitivity modeling with age, sex, and inhaled corticosteroid use as covariates; and (iii) joint consideration of FDR and enrichment ratio to reduce reliance on any single statistic. Directionality and pathway-level inferences remained unchanged across checks.

Summary. The High-IL-33 lipidome was marked by coordinated upregulation of TG/CL/PE/DG/PC/PS and KEGG enrichment in fat digestion and absorption, adipocyte lipolysis regulation, NF- κ B signaling, and Th1/Th2 differentiation. These features correlated with indicators of suboptimal control and atopy, providing a metabolic and structural context for integration with proteomic signals (Endocytosis/cAMP/Neurotrophin/Sphingolipid) and supporting a mechanistic axis linking IL-33 to membrane remodeling and immune activation.

3.3 Proteomic analysis

3.31 Global proteomic profile

Using TMT-labeled quantitative mass spectrometry on serum from the high- and low-IL-33 groups, we identified 18,883 peptides and 2,100 proteins, of which 2,098 were quantifiable (FDR <1% at both peptide and protein levels). Sample-level principal component analysis (PCA) indicated a trend toward separation between groups in overall protein expression, with no evident batch effect (Fig 3A; QC in Fig. S4). This pattern mirrors the groupwise divergence observed in the global lipidome (Fig 3A), suggesting that differences in IL-33 levels are closely associated with alterations in the circulating proteome.

3.32 Identification of differentially expressed proteins

In the proteomic comparison between the high- and low-IL-33 groups (n=6 per group), 942 differentially expressed proteins were identified, including 190 upregulated and 20 downregulated proteins (selection criteria: $FC \geq 2.0$ or ≤ 0.50 , FDR < 0.05). Representative proteins included ENPP4, STAM2, CIPBP, PRPSAP2, RIMOC1, NT5C2, PSMD8, KTN1, ACAA1, and VPS25 (Table S3; Fig 3A–C).

Functionally, these proteins clustered into three principal categories:

1. Metabolic reprogramming–related proteins: ENPP4, PRPSAP2, NT5C2, and ACAA1 are primarily involved in nucleotide metabolism and fatty-acid β -oxidation, indicating enhanced substrate utilization and energy supply in the high-IL-33 group. This aligns with lipidomic enrichment in triglyceride metabolism and regulation of lipolysis in adipocytes, supporting coordinated metabolic remodeling.
2. Membrane dynamics and vesicular transport: STAM2, KTN1, and VPS25 regulate receptor-mediated endocytosis, cytoskeleton interactions, and endosome-to-lysosome trafficking, respectively. Their upregulation suggests heightened vesicular transport and receptor recycling, consonant with lipidomic indications of altered membrane dynamics (elevated PC/PE/CL with reduced GM3).
3. Signal transduction and immune regulation: PSMD8 (a proteasome subunit) and CIPBP are linked to protein degradation and transcriptional regulation, whereas RIMOC1 participates in vesicular trafficking and synapse-related signaling. Collectively, these molecules may facilitate NF- κ B activation and T-cell differentiation, in agreement with lipidomic enrichment of NF- κ B and Th1/Th2/Th17 pathways.

Together, the differential proteins delineate changes across three interconnected layers—metabolic reprogramming (augmented energy supply), membrane/vesicular remodeling (enhanced endocytosis and trafficking), and signal amplification (NF- κ B activation with strengthened immune effector programs). Integrated with the lipidomics, these findings support a mechanistic cascade: elevated IL-33 → lipid metabolic remodeling → upregulation of key proteins → signal amplification → intensified immuno-inflammation → poorer asthma control (Fig 3D).

3.33 Functional and pathway enrichment analysis

KEGG enrichment of differentially expressed proteins (DEPs) demonstrated significant over-representation of the cAMP signaling pathway, Neurotrophin signaling pathway, Endocytosis, and the Sphingolipid signaling pathway (FDR < 0.05; Fig 3D). These pathways are integral to inflammatory amplification, metabolic reprogramming, and immune disequilibrium.

(1) cAMP signaling. DEP enrichment indicates activation of the canonical GPCR–adenylyl cyclase–PKA axis in the high-IL-33 group. As a second messenger, cAMP regulates adipocyte lipolysis and exhibits cross-talk with inflammatory cascades such as NF- κ B and MAPK. Together with lipidomic upregulation of triglyceride metabolism and regulation of lipolysis in adipocytes, these findings suggest that metabolic products (e.g., free fatty acids) interact with cAMP signaling to fuel immune-cell energetics and intensify inflammatory responses.

(2) Neurotrophin signaling. This pathway encompasses Trk receptor–PI3K/AKT–MAPK cascades that govern neuronal survival, synaptic plasticity, and neuro–immune interactions. Its enrichment in the high-IL-33 group points to potentiated neuro–immune crosstalk within the airways, consistent with neurogenic inflammation and heightened airway hyperresponsiveness. This provides molecular support for a link between IL-33–driven immune inflammation and neural dysregulation.

(3) Endocytosis. Multiple DEPs participate in receptor internalization, vesicular trafficking, and endosome-to-lysosome transport. This enrichment aligns with lipidomic evidence of altered membrane dynamics (increased PC/PE/CL with decreased GM3), indicating that membrane remodeling furnishes the physical basis for dynamic receptor control. Enhanced endocytosis and recycling may prolong the duration of inflammatory signaling and amplify IL-33–driven immune effects.

(4) Sphingolipid signaling. Sphingolipid mediators (e.g., ceramide and sphingosine-1-phosphate, S1P) regulate apoptosis, inflammation, and immune-cell trafficking. Enrichment of this pathway is concordant with lipidomic observation of reduced GM3, implying rewired sphingolipid regulation that may lower immune tolerance and magnify inflammatory responses.

Collectively, proteomic enrichment supports systemic enhancement across four axes in the high-IL-33 group—second-messenger amplification (cAMP), neuro–immune interaction (Neurotrophin), receptor internalization and cycling (Endocytosis), and membrane lipid–signal coupling (Sphingolipid). These findings provide functional corroboration for lipidomics-defined membrane remodeling and immune-pathway activation, converging on a mechanistic chain in which elevated IL-33 drives metabolic remodeling → membrane-dynamics reprogramming → signal amplification → intensified immuno-inflammation.

3.34 Associations among the proteome, lipidome, and clinical phenotypes

Integrated analyses showed that proteomic enrichment of the cAMP and Endocytosis pathways paralleled lipidomic increases in PC, PE, and CL, jointly indicating membrane-lipid remodeling with attendant signal amplification. In contrast, downregulated proteins related to energy

metabolism/mitochondrial function aligned with decreased SM and higher peripheral eosinophil percentages.

Correlation analyses further revealed that modules of differentially expressed proteins were positively associated with Asthma Control Questionnaire (ACQ) scores and total IgE, whereas proteins involved in sustaining energy metabolism were negatively associated with asthma control (i.e., lower ACQ) (Fig 4E).

In sum, the proteomic data indicate that elevated IL-33 primarily enhances vesicular trafficking, cAMP signaling, and neuro-immune crosstalk to amplify inflammatory signals, concomitant with impaired energy metabolism. Together with the lipidomic findings, these results support a mechanistic sequence in which IL-33 amplifies immune disequilibrium via coordinated lipid-protein interactions, culminating in poorer asthma control.

3.4 Integrated lipidomic-proteomic analysis

To determine whether the IL-33-related shifts in circulating lipids and serum proteins reflect two parallel, layer-restricted responses or a single, convergent IL-33-driven program, we conducted a joint analysis of the lipidomic and proteomic datasets generated under the same high- versus low-IL-33 stratification.

At the pathway level, the two omics layers showed marked concordance: 42 KEGG pathways were enriched by both differential lipids and differential proteins (Fig 4A), while the remaining pathways were specific to one layer. Importantly, these shared pathways did not distribute randomly but aggregated into two mechanistic clusters:

1. immune and inflammatory signalling, including Th1/Th2 cell differentiation, NF- κ B signalling and Fc γ R-mediated phagocytosis (Fig 4B).
2. membrane-, cytoskeleton- and vesicle-handling modules, such as endocytosis, regulation of the actin cytoskeleton, focal adhesion, tight junction and adherens junction (Fig 4B).

This pattern indicates that lipid and protein alterations in the IL33 high subgroup do not act independently but converge on an immune axis that requires both a permissive and reconfigured membrane platform and an activated system for receptor processing and vesicle transport.

Cross-omics correlation analysis further supported this convergence. Proteins assigned to the actin-adhesion-endocytic submodules (e.g. ARPC3, TAGLN2, RAC1, ZYX, FLNA, TLN1, VASP) showed FDR-significant positive correlations with lipid classes elevated in IL-33-high children, including PC/PE species, cardiolipins (CL) and selected sphingolipids, whereas several SM-containing species exhibited inverse trends (Fig 4C). This cross-layer architecture is consistent with a model in which IL-33-associated membrane remodelling (PC/PE/CL \uparrow , SM \downarrow) generates a more fluid, clustering-competent surface, while the up-regulated endocytic and actin-remodelling proteins ensure efficient receptor turnover and vesicle trafficking on that surface.

We next assessed the clinical relevance of these integrated molecular signals. Key proteins within the endocytosis/ESCRT/vesicle cluster (STAM2, VPS25, VAMP3, VAMP8, NT5C2, PSMD8, CIRBP) were positively correlated with asthma control questionnaire (ACQ) scores and, to a lesser degree, with serum IgE and peripheral blood eosinophil percentage, whereas the β -oxidation enzyme ACAA1 showed negative correlations with the same outcomes (Fig 4D). In parallel, the principal differential lipids—particularly PC/PE/CL species—displayed correlation profiles in the same clinical direction (higher ACQ, higher IgE, higher eosinophils), again in contrast to several SM-related species (Fig 4E). The fact that both omics layers reproduce the same clinical gradients argues that the IL-33-responsive signature is not purely biochemical but reflects in vivo disease activity and type-2-skewed inflammation.

Finally, when these findings are interpreted in the context of the IL-33/ST2–cAMP/PKA–NF- κ B framework (Fig 4F), a coherent mechanism emerges: IL-33/ST2 engagement in paediatric asthma is accompanied by (i) a shift from SM-rich microdomains toward PC/CL-enriched, more compliant membranes; (ii) a coordinated up-regulation of vesicle/ESCRT and actin-remodelling proteins that facilitate receptor internalisation, recycling and signal persistence; and (iii) downstream activation of NF- κ B and Th1/Th2/Th17 programmes, together with a metabolic down-tuning exemplified by ACAA1 reduction and PPARA/SREBF1-linked lipid rewiring. This dual-arm model provides a mechanistic basis for the clinical phenotype observed in the IL-33-high subgroup—worse asthma control, higher total IgE and higher eosinophil percentages—and aligns with the integrated scheme illustrated in the uploaded figures.

3.5 qPCR validation of key pathways

To validate the enrichment results from the lipidomic and proteomic analyses—particularly the shared enrichment of the NF- κ B signaling pathway—we performed a targeted qPCR panel focusing on key nodes of the NF- κ B/Th polarization axis, cAMP signaling, endocytosis, sphingolipid metabolism, and lipolysis/energy regulation. The validation panel included RELA, NFKBIA, GATA3, TBX21, PRKACA, STAM2, SPHK1, and LIPE, with ADCY6, S1PR1, and ACAA1 added to broaden pathway coverage.

Compared with the low-IL-33 group, children in the high-IL-33 group showed significantly higher transcript levels of RELA, GATA3, PRKACA, STAM2, SPHK1, and LIPE, whereas NFKBIA was down-regulated (all FDR < 0.05). ADCY6, S1PR1, and ACAA1 exhibited trends consistent with the directions observed in the cross-omics analysis (Fig 5A).

At the gene–clinical correlation level, expression of RELA, IL1B, GATA3, PRKACA, STAM2, SPHK1, and LIPE was positively correlated with asthma control questionnaire (ACQ) scores, total IgE, and peripheral eosinophil percentage, whereas NFKBIA and TBX21 were negatively correlated with these clinical endpoints. In parallel, genes reflecting vesicular and second-messenger processes (such as PRKACA, STAM2, and ADCY6) were associated with the lipidomic signature of membrane remodeling, characterized by increases in PC, PE, and CL and decreases in GM3 (Fig 5B–C). Taken together, these transcriptional data independently support the proposed sequence whereby IL-33 elevation drives membrane lipid remodeling, augments endocytic and second-messenger pathways, and ultimately

promotes NF- κ B activation and Th2-skewed responses, which in turn associate with poorer clinical control. This is fully concordant with the directions indicated by the integrated multi-omics enrichment.

Discussion

The clinical heterogeneity of asthma reflects endotypes driven by intersecting immune and metabolic processes[24, 25]. As an epithelial-derived alarmin, interleukin-33 (IL-33) signals through the ST2 receptor to integrate innate and adaptive immunity and is considered pivotal in the initiation and persistence of pediatric asthma[25–27]. Using serum IL-33 as a stratification anchor, this study delineates downstream molecular features across lipidomic and proteomic layers and relates them to disease control and atopic indices, with the overarching goal of defining a testable “immune–metabolic coupling” framework[28, 29].

First, the high-IL-33 group exhibited a clear lipid-remodeling signature: global increases in TG, CL, PE, DG, PC, and PS. KEGG analyses highlighted enrichment in fat digestion and absorption, regulation of lipolysis in adipocytes, NF- κ B signaling, and Th1/Th2 differentiation. Mechanistically, enhanced lipid uptake and mobilization provide substrates for membrane composition and energy supply; concomitant increases in PC/PE/CL and a decline in selected SM species suggest reprogramming of membrane microdomains and receptor environments, favoring signalosome assembly and receptor clustering, thereby lowering the inflammatory activation threshold and prolonging signal residence[30]. Proteomics corroborated these findings, with upregulation of Endocytosis, cAMP, Neurotrophin, and Sphingolipid pathways, pointing to amplification of vesicular trafficking and second-messenger signaling and cross-talk with the NF- κ B axis and T-helper polarization[31–33]. Taken together, the data support a coherent biological cascade: elevated IL-33 → membrane-lipid remodeling → vesicular/second-messenger amplification → NF- κ B activation and Th polarization.

Second, the molecular features aligned with clinical phenotypes. Multiple upregulated lipid classes and their pathway enrichment scores correlated positively with ACQ score, total IgE, and peripheral eosinophil percentage, indicating that “structural–functional” remodeling tracks with poor control and heightened atopy[23, 34, 35]. These results have immediate clinical implications:

(1) Stratification and prognosis.

Combining IL-33 levels with a lipid–protein fingerprint (PC/PE/CL \uparrow , SM \downarrow , and Endocytosis/cAMP features) yields a quantifiable endotype that complements symptom scales in outpatient settings for risk stratification, exacerbation prediction, and individualized follow-up; on this basis, a practical “IL-33–lipid–transport” composite index could identify an “activated membrane–transport” phenotype[23, 36].

(2) Therapy selection and sequencing.

The fingerprint informs the choice and timing of anti-IL-33/anti-ST2 and type-2 biologics (anti-IL-5/anti-IL-4R α) and supports exploration of combination approaches (IL-33 blockade plus lipid-pathway

modulation and microdomain-targeted cAMP control, with or without cautious inhibition of Endocytosis/ESCRT) to raise activation thresholds and shorten signal persistence[37].

Strengths of this work include clinically actionable stratification by IL-33, dual-omics concordance with qPCR validation, rigorous BH-FDR control, and pathway/network-level interpretation that avoids over-extrapolation from single molecules. Limitations include a modest sample size and cross-sectional design, which constrain causal inference; potential underdetection of membrane-associated proteins in serum proteomics due to high-abundance species; and the absence of cellular or in vivo functional assays[38, 39]. These strengths and limitations are consistent with prior omics-based asthma studies[23]. Future studies should comprise large, longitudinal cohorts with external validation; ex vivo stimulation and blockade experiments in peripheral immune cells; and mediation/path analysis to test the stability and translational promise of the pathway “IL-33 → molecular modules → clinical outcomes.”

In summary, elevated IL-33 in pediatric asthma coincides with coordinated lipid–protein reprogramming—membrane-lipid remodeling coupled to vesicular/second-messenger amplification—biasing NF-κB activation and T-helper responses, and paralleling poor control and augmented atopy. This molecular fingerprint shows utility for stratification and monitoring and nominates lipid metabolism and downstream inflammatory signaling as tractable therapeutic targets meriting prospective evaluation within clinical pathways[22, 40].

Conclusion

Using a multi-omics approach, this study delineates potential molecular mechanisms by which IL-33 operates in pediatric asthma. Lipidomics revealed marked increases in PC, PE, and CL with enrichment in NF-κB signaling and Th1/Th2/Th17 differentiation pathways, implicating membrane-lipid remodeling in the proximal activation of inflammatory signaling. Proteomics further demonstrated enhanced SNARE-mediated vesicular transport, cAMP signaling, and endocytosis, providing functional support for receptor clustering, signal transduction, and immune amplification downstream of membrane changes.

Integrated analyses indicate that IL-33 elevation couples lipid metabolic abnormalities with upregulation of vesicular transport and signaling proteins to amplify immuno-inflammatory cascades, in close agreement with clinical features of poorer asthma control, higher total IgE, and increased eosinophil percentages.

Together, these data support a sequential model—metabolic remodeling → membrane architectural change → signal amplification → immune disequilibrium—as a key molecular basis for suboptimal asthma control in children. Differential lipid species and the highlighted protein pathways may serve as candidate biomarkers and actionable targets, providing a rationale for precision assessment and intervention in IL-33–related pediatric asthma.

Declarations

Acknowledgements

Thanks to the lab members for valuable discussions and suggestions.

Author Contribution

Tong Xiao and Min Liu conceived and designed the projects. Yingtan Yu performed all studies, analysed data and wrote the manuscript. LWanying Liu, Tongtong Wang, Hui Wang and Tianzhi Chang performed some of the experiments and data analysis. All authors read and approved the final manuscript.

Funding

This study was supported by Jiangsu Provincial Medical Association Pediatric Special Research Project (SYH-32034-0074, 20230021); Wuxi Science and Technology Bureau "Taihu Light" Technical Research Project (Y20222005).

Availability of data and materials

The datasets generated during and/or analysed during the current study are available from the corresponding author on reasonable request.

Ethics approval and consent to participate

The study was conducted in strict accordance with the protocol approved by the Ethics Committee of the Affiliated Hospital of Jiangnan University (LS2022112) and with the informed consent of all participants.

Consent for publication

Not applicable.

Competing interests

The authors declare that they have no financial or non-financial competing interests relevant to the work described in this manuscript. The study was conducted in an academic setting, no commercial entity had any role in the study design, data acquisition, data analysis, interpretation of the results, writing of the manuscript, or the decision to submit it for publication. The authors have no patents, patent applications, consultancy, stock ownership, speakers' fees, or other relationships that could be perceived to influence the results or discussion of this paper.

References

1. Asher, M. I. et al. Worldwide trends in the burden of asthma symptoms in school-aged children: Global Asthma Network Phase I cross-sectional study. *Lancet* **398** (10311), 1569–1580 (2021).

2. Foppiano, F. & Schaub, B. Childhood asthma phenotypes and endotypes: a glance into the mosaic. *Mol. Cell. Pediatr.* **10** (1), 9 (2023).
3. Papadopoulos, N. G. et al. Type 2 Inflammation and Asthma in Children: A Narrative Review. *J. Allergy Clin. Immunol. Pract.* **12** (9), 2310–2324 (2024).
4. Habte, B. M., Beyene, K. A., Patel, S. A., Fenta, T. G. & Fitzpatrick, A. M. Asthma Control and Associated Factors Among Children with Current Asthma - Findings from the 2019 Child Behavioral Risk Factor Surveillance System - Asthma Call-Back Survey. *J. Asthma Allergy.* **17**, 611–620 (2024).
5. Liu, A. H. et al. Status of asthma control in pediatric primary care: results from the pediatric Asthma Control Characteristics and Prevalence Survey Study (ACCESS). *J. Pediatr.* **157** (2), 276–281e273 (2010).
6. Bacharier, L. B. et al. Blood eosinophils and fractional exhaled nitric oxide are prognostic and predictive biomarkers in childhood asthma. *J. Allergy Clin. Immunol.* **154** (1), 101–110 (2024).
7. Qin, Z. et al. Immunometabolism in the pathogenesis of asthma. *Immunology* **171** (1), 1–17 (2024).
8. Liew, F. Y., Girard, J. P. & Turnquist, H. R. Interleukin-33 in health and disease. *Nat. Rev. Immunol.* **16** (11), 676–689 (2016).
9. Cayrol, C. & Girard, J. P. Interleukin-33 (IL-33): A critical review of its biology and the mechanisms involved in its release as a potent extracellular cytokine. *Cytokine* **156**, 155891 (2022).
10. Oh, K. et al. Airway epithelial cells initiate the allergen response through transglutaminase 2 by inducing IL-33 expression and a subsequent Th2 response. *Respir. Res.* **14** (1), 35 (2013).
11. Oh, K. et al. Airway epithelial cells initiate the allergen response through transglutaminase 2 by inducing IL-33 expression and a subsequent Th2 response. *Respir Res.* **14** (1), 35 (2013).
12. Maffeis, L. et al. Cytokines Profile and Lung Function in Children with Obesity and Asthma: A Case Control Study. *Child. (Basel)*; **9**(10). (2022).
13. Daley-Yates, P., Keppler, B., Baines, A., Bardsley, G. & Fingleton, J. Metabolomic changes related to airway inflammation, asthma pathogenesis and systemic activity following inhaled fluticasone furoate/vilanterol: a randomized controlled trial. *Respir Res.* **23** (1), 258 (2022).
14. Cheng, H. & Zheng, Y. Advances in macrophage and T cell metabolic reprogramming and immunotherapy in the tumor microenvironment. *PeerJ* **12**, e16825 (2024).
15. van Deventer, S., Arp, A. B. & van Sriel, A. B. Dynamic Plasma Membrane Organization: A Complex Symphony. *Trends Cell. Biol.* **31** (2), 119–129 (2021).
16. Rother, N. et al. Acid ceramidase regulates innate immune memory. *Cell. Rep.* **42** (12), 113458 (2023).
17. Price, M. M. et al. A specific sphingosine kinase 1 inhibitor attenuates airway hyperresponsiveness and inflammation in a mast cell-dependent murine model of allergic asthma. *J. Allergy Clin. Immunol.* **131** (2), 501–511e501 (2013).
18. Yang, J. et al. Sphingosine-1-phosphate signaling in respiratory diseases: mechanisms and therapeutic perspectives. *Int. Immunopharmacol.* **166**, 115578 (2025).

19. Terashita, T. et al. Administration of JTE013 abrogates experimental asthma by regulating proinflammatory cytokine production from bronchial epithelial cells. *Respir Res.* **17** (1), 146 (2016).
20. Nicolaou, A., Mauro, C., Urquhart, P. & Marelli-Berg, F. Polyunsaturated Fatty Acid-derived lipid mediators and T cell function. *Front. Immunol.* **5**, 75 (2014).
21. Prinz, W. A. Bridging the gap: membrane contact sites in signaling, metabolism, and organelle dynamics. *J. Cell. Biol.* **205** (6), 759–769 (2014).
22. Liu, S. et al. Multi-omics identifies severe asthma endotypes linked to Streptococcus dysbiosis and lipid metabolic dysregulation. *World Allergy Organ. J.* **18** (11), 101132 (2025).
23. Brandsma, J. et al. Stratification of asthma by lipidomic profiling of induced sputum supernatant. *J. Allergy Clin. Immunol.* **152** (1), 117–125 (2023).
24. Kuruvilla, M. E., Lee, F. E. & Lee, G. B. Understanding Asthma Phenotypes, Endotypes, and Mechanisms of Disease. *Clin. Rev. Allergy Immunol.* **56** (2), 219–233 (2019).
25. Maggi, E., Parronchi, P., Azzarone, B. G. & Moretta, L. A pathogenic integrated view explaining the different endotypes of asthma and allergic disorders. *Allergy* **77** (11), 3267–3292 (2022).
26. Saglani, S. et al. IL-33 promotes airway remodeling in pediatric patients with severe steroid-resistant asthma. *J. Allergy Clin. Immunol.* **132** (3), 676–685e613 (2013).
27. Aldossary, H., Karkout, R., Couto, K., Labrie, L. & Fixman, E. D. IL-33-experienced group 2 innate lymphoid cells in the lung are poised to enhance type 2 inflammation selectively in adult female mice. *Respir Res.* **25** (1), 427 (2024).
28. Momen, T. et al. Comparison of Interleukin-33 Serum Levels in Asthmatic Patients with a Control Group and Relation with the Severity of the Disease. *Int. J. Prev. Med.* **8**, 65 (2017).
29. Yang, Q. et al. Serum interleukin-33 combined with FEF75% z-score and FeNO improves the diagnostic accuracy of asthma in children. *J. Pediatr. (Rio J).* **100** (1), 81–87 (2024).
30. Kraft, M. L. Sphingolipid Organization in the Plasma Membrane and the Mechanisms That Influence It. *Front. Cell. Dev. Biol.* **4**, 154 (2016).
31. Hara, R. et al. Potential asthma biomarkers identified by nontargeted proteomics of extracellular vesicles in exhaled breath condensate. *J. Allergy Clin. Immunol. Glob.* **4** (2), 100432 (2025).
32. Sundar, I. K., Li, D. & Rahman, I. Correction to Proteomic Analysis of Plasma-Derived Extracellular Vesicles in Smokers and Patients with Chronic Obstructive Pulmonary Disease. *ACS Omega.* **10** (19), 20058 (2025).
33. Chinn, A. M. & Insel, P. A. Cyclic AMP in dendritic cells: A novel potential target for disease-modifying agents in asthma and other allergic disorders. *Br. J. Pharmacol.* **177** (15), 3363–3377 (2020).
34. Jiang, T. et al. Lipid metabolism and identification of biomarkers in asthma by lipidomic analysis. *Biochim. Biophys. Acta Mol. Cell. Biol. Lipids.* **1866** (2), 158853 (2021).
35. Liu, Y. et al. Sputum Metabolomic Profiling Reveals Metabolic Pathways and Signatures Associated With Inflammatory Phenotypes in Patients With Asthma. *Allergy Asthma Immunol. Res.* **14** (4), 393–411 (2022).

36. Zhao, R., Shi, Y., Liu, N. & Li, B. Elevated levels of interleukin-33 are associated with asthma: A meta-analysis. *Immun. Inflamm. Dis.* **11** (4), e842 (2023).

37. Kelsen, S. G. et al. Astegolimab (anti-ST2) efficacy and safety in adults with severe asthma: A randomized clinical trial. *J. Allergy Clin. Immunol.* **148** (3), 790–798 (2021).

38. Watanabe, M. et al. Serum sST2 levels predict severe exacerbation of asthma. *Respir Res.* **19** (1), 169 (2018).

39. Aebersold, R. & Mann, M. Mass-spectrometric exploration of proteome structure and function. *Nature* **537** (7620), 347–355 (2016).

40. Zhang, W., Zhang, Y., Li, L., Chen, R. & Shi, F. Unraveling heterogeneity and treatment of asthma through integrating multi-omics data. *Front. Allergy.* **5**, 1496392 (2024).

Figures

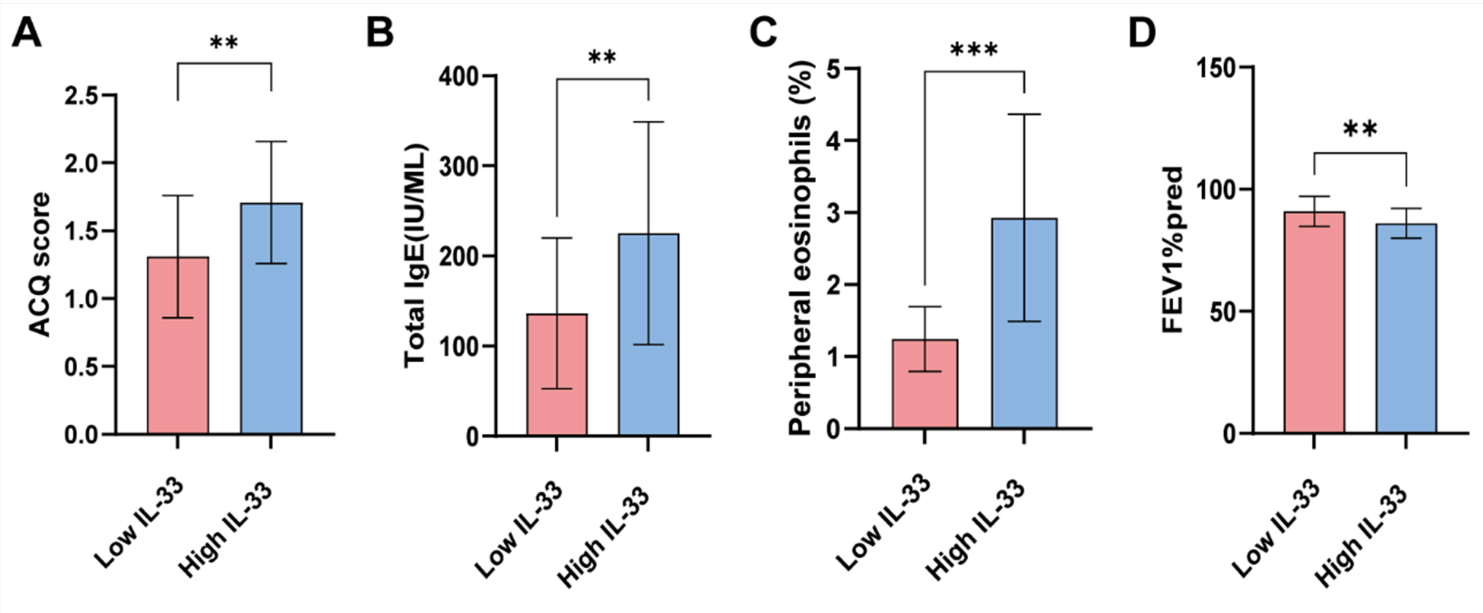


Figure 1

Clinical characteristics of pediatric asthma patients stratified by serum IL-33.

Bar/box plots show groupwise comparisons between the Low IL-33 group (n = 30) and the High IL-33 group (n = 30) for (A) ACQ score, (B) total IgE, (C) peripheral blood eosinophil percentage, and (D) FEV₁ % predicted. Children with higher serum IL-33 displayed poorer asthma control (higher ACQ), higher allergic burden (higher total IgE), greater eosinophilic inflammation, and lower lung function (lower FEV₁ %pred) than those with low IL-33. p-values are from independent-samples t-tests; **p < 0.01, ***p < 0.001. Error bars represent SD.

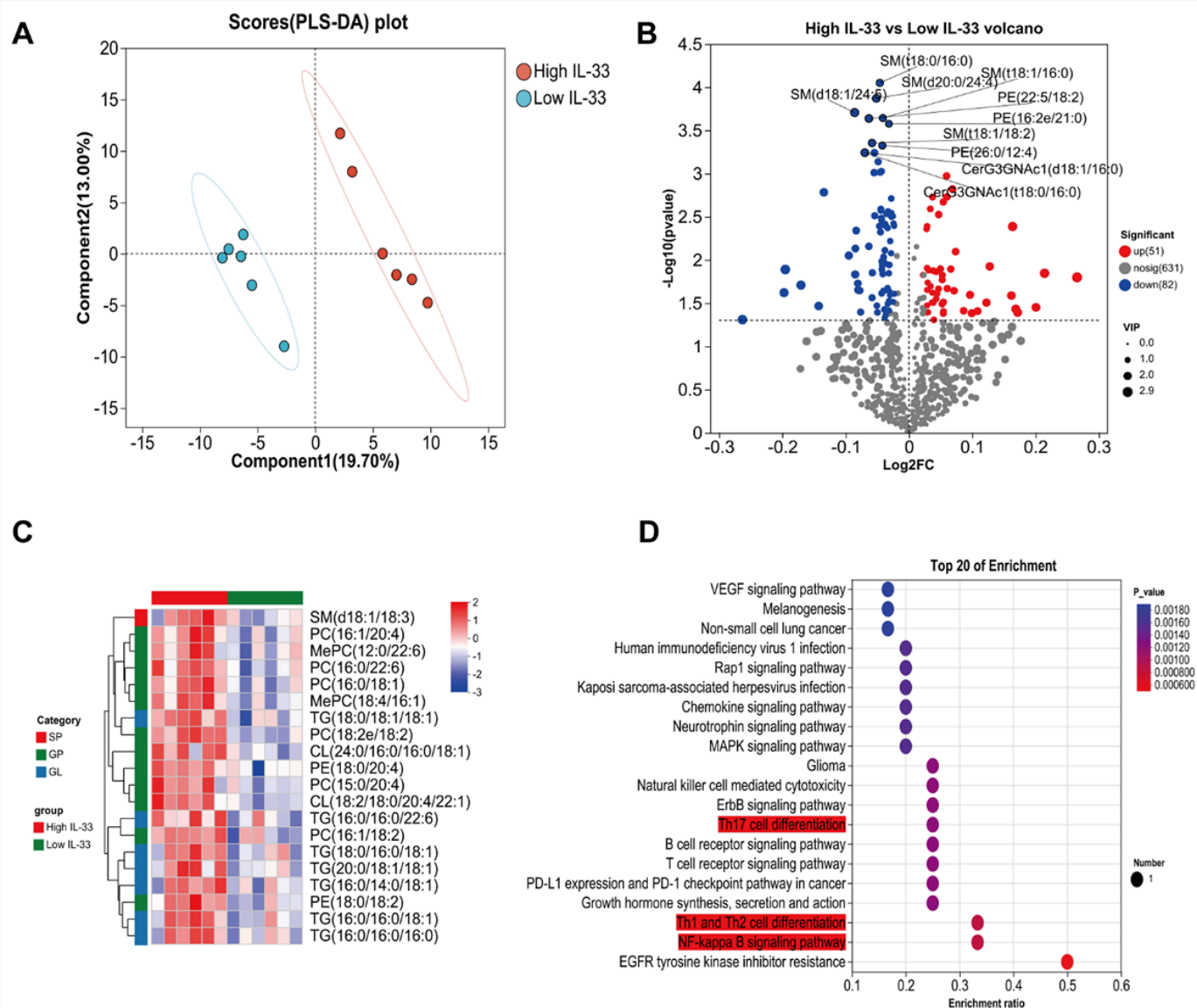


Figure 2

Differential serum lipid profiles between high and low IL-33 pediatric asthma groups.

(A) PLS-DA scores plot showing clear separation of the high IL-33 group (red) from the low IL-33 group (blue), indicating distinct lipidomic signatures. (B) Volcano plot of differential lipids (high IL-33 vs. low IL-33); red dots denote significantly upregulated species in the high IL-33 group, blue dots denote downregulated species, and dot size reflects VIP values. Representative species (e.g. SM, PC/PE, Cer/GalCer) are annotated. (C) Hierarchical clustering heatmap of selected differential lipids, grouped by lipid class (SM, SP, GP, GL); most high-IL-33 samples cluster together and are characterized by higher PC/PE/CL/TG and lower SM species. (D) KEGG pathway enrichment of differential lipids (top 20 pathways), highlighting immune- and inflammation-related pathways, including NF- κ B signaling, Th1/Th2/Th17 cell differentiation, and natural killer cell-mediated cytotoxicity, supporting convergence of IL-33-associated lipid remodeling on immune pathways.

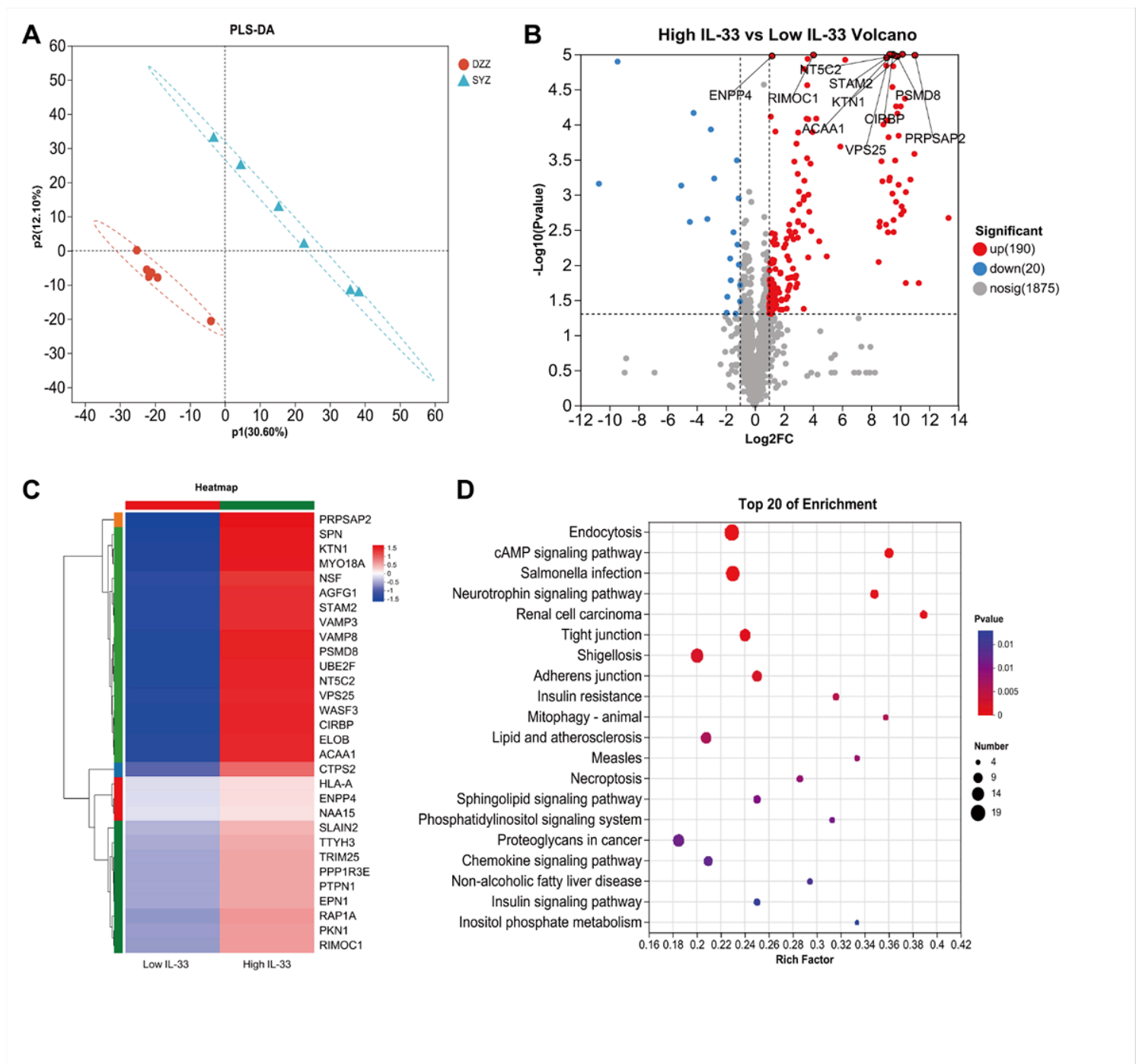


Figure 3

Proteomic signatures associated with high serum IL-33 in pediatric asthma.(A) PLS-DA score plot showing clear separation between the low IL-33 group and the high IL-33 group, indicating distinct serum proteomic profiles.(B) Volcano plot of differentially expressed proteins (high IL-33 vs. low IL-33). Red dots denote significantly upregulated proteins (n = 190), blue dots denote downregulated proteins (n = 20), and grey dots represent non-significant proteins (n = 1,875). Representative IL-33-related proteins (e.g. STAM2, VPS25, NT5C2, KTN1, PSMB8, ACAA1, ENPP4) are annotated.(C) Heatmap of selected differentially expressed proteins, clustered by expression pattern. Most high-IL-33 samples are characterized by higher abundance of proteins involved in vesicular transport, ESCRT components, and

immune regulation.(D) KEGG pathway enrichment analysis of the differentially expressed proteins (top 20 pathways). Endocytosis, cAMP signaling, neurotrophin signaling, tight/adherens junctions, sphingolipid signaling, and phosphatidylinositol signaling were among the most significantly enriched pathways, indicating that IL-33–related proteomic changes converge on vesicle trafficking and second-messenger/immune pathways. P-values were adjusted for multiple testing.

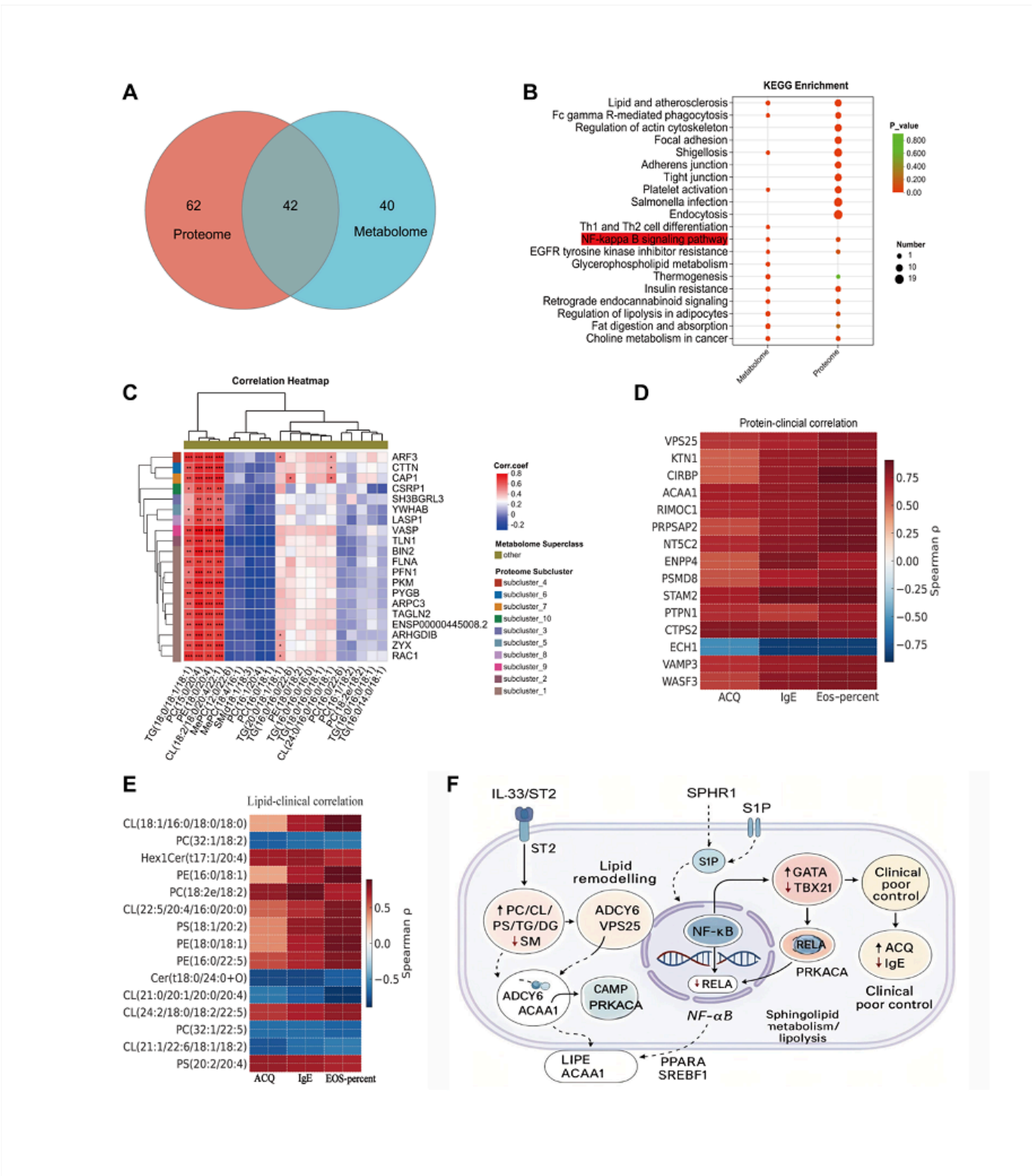


Figure 4

Integrated proteomic–lipidomic analysis and proposed IL-33–driven mechanism.

(A) Venn diagram showing the overlap between differentially expressed proteins (Proteome, n = 62) and differential lipid/metabolite features (Metabolome, n = 40); 42 molecules/pathways were shared by both layers.

(B) KEGG enrichment of proteome-specific, shared, and metabolome-specific signals. Pathways related to membrane dynamics and inflammation (e.g. regulation of actin cytoskeleton, endocytosis, adherens/tight junctions) as well as immune pathways (Th1 and Th2 cell differentiation, NF-κB signaling, pathogen response) were simultaneously enriched, indicating convergence of the two omics layers. Dot size represents the number of mapped molecules; color denotes adjusted p value.

(C) Correlation heatmap linking representative proteins (e.g. ARF3, CTTN, CAP1, STAM2, TAGLN2, RAC1) with lipid/metabolite subclasses. Positive associations (red) highlight coordinated changes between vesicle/actin/ESCRT-related proteins and lipid subclasses enriched in the high-IL-33 group.

(D) Schematic model summarizing the IL-33/ST2–S1P axis: IL-33–induced lipid remodeling (↑PC/CL/PS/TG/DG, ↓SM) promotes ADCY6–cAMP–PRKACA signaling and ESCRT/VPS25-mediated endocytosis, which in turn augments NF-κB (RELA) activity and Th2 skewing (GATA3↑, TBX21↓), ultimately leading to poor clinical control (↑ACQ, ↑IgE).

(E) Protein–clinical correlation matrix showing that VPS25, KTN1, CIRBP, PRPSAP2 and other vesicle/immune-related proteins correlate positively with ACQ, total IgE and blood eosinophil percentage, whereas ACAA1 and several metabolic proteins show inverse relationships. Correlations were calculated using Spearman's ρ and visualized after multiple-testing adjustment.

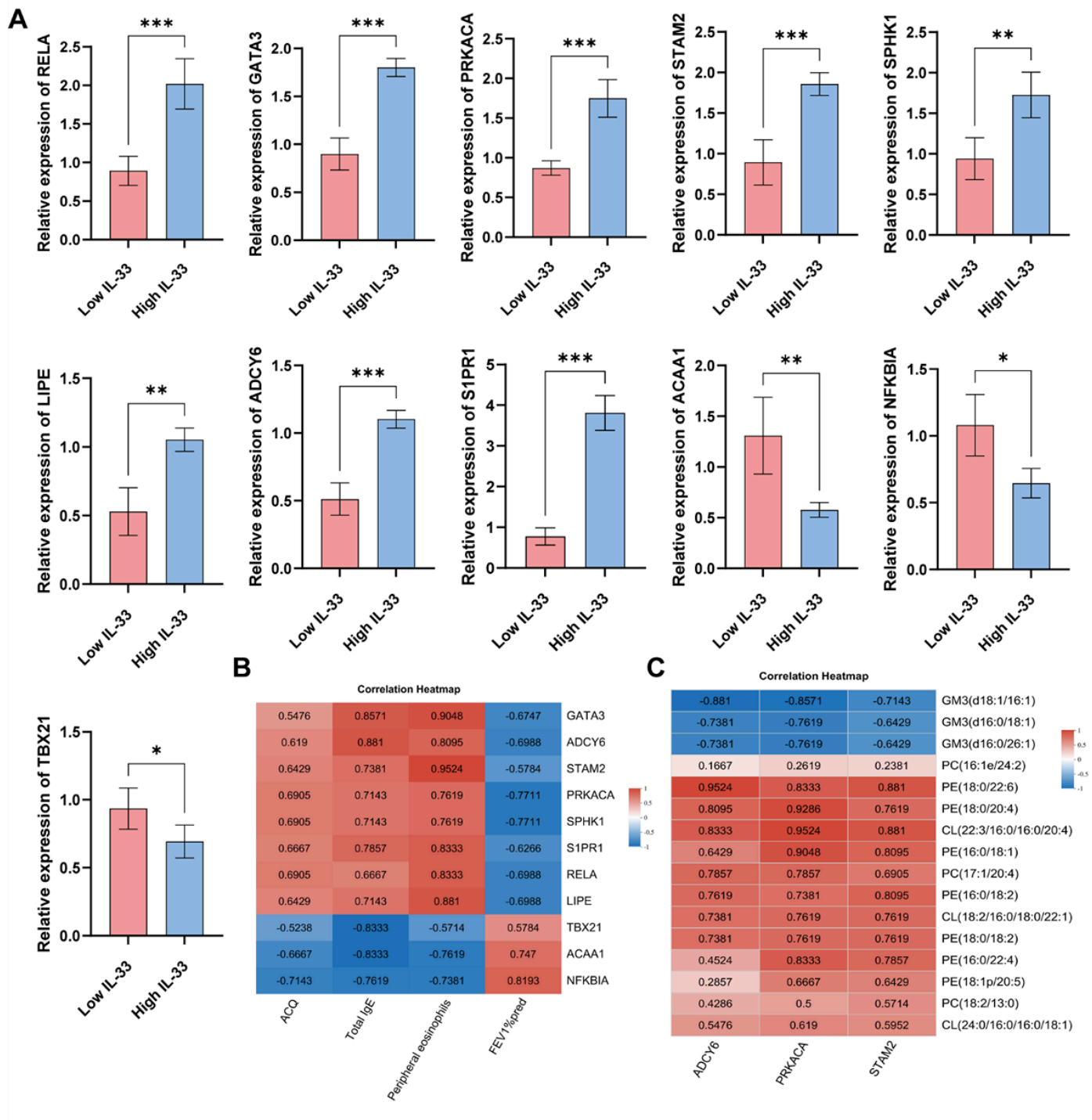


Figure 5

qPCR validation of the cross-omics intersecting pathway (NF- κ B axis)

(A) Target panel gene expression in High vs. Low IL-33 groups (box plots with overlaid points, displayed as $2^{-\Delta Ct}$ or $2^{-\Delta\Delta Ct}$): RELA, GATA3, PRKACA, STAM2, SPHK1, and LIPE are significantly increased in the High IL-33 group, whereas NFKBIA is decreased; supplemental genes ADCY6, S1PR1, and ACAA1 change in directions consistent with the cross-omics findings (all Benjamini–Hochberg FDR adjusted,

FDR < 0.05). (B) Gene-level correlations: expression of RELA, IL1B, GATA3, PRKACA, STAM2, SPHK1, and LIPE correlates positively with ACQ score, total IgE, and peripheral blood eosinophil percentage, whereas NFKBIA and TBX21 correlate negatively (Spearman's ρ shown, FDR < 0.05). (C) Correlations between vesicular/second-messenger genes (e.g., PRKACA, STAM2, ADCY6) and lipidomic features of membrane remodeling (upregulated PC/PE/CL, downregulated GM3) (Spearman's ρ , FDR < 0.05), indicating coupling of lipid changes with the endocytosis–cAMP program converging on the NF- κ B/Th axis. Statistics: tests performed on Δ Ct values (two-sided); multiple comparisons for genes and correlations controlled by Benjamini–Hochberg FDR; each sample run in technical triplicate. Sample size: n = 60 (High IL-33 = 4, Low IL-33 = 4).

Supplementary Files

This is a list of supplementary files associated with this preprint. Click to download.

- [Fig.S1S4.docx](#)
- [TableS1.xlsx](#)
- [TableS2.Detailedtableofdifferentiallipids.xlsx](#)
- [TableS3.Detailedtableofdifferentialproteins.xlsx](#)